On the origin of chevron marks and striated grooves, and their use in predicting mud bed rheology

McGowan, Dylan; Salian, Amisha; Baas, Jaco; Peakall, Jeff; Best, Jim

Sedimentology

SEDIMENTOLOGY

the Journal of the
International Association of Sedimentologists

On the origin of chevron marks and striated grooves, and their use in predicting mud bed rheology

SCHOLARONE™
Manuscripts

On the origin of chevron marks and striated grooves, and their use in predicting mud bed rheology

Dylan McGowan[1], Amisha Salian[1], Jaco H. Baas[1], Jeff Peakall[2], Jim Best[3]

[1] School of Ocean Sciences, Bangor University, Menai Bridge, LL59 5AB, Wales, UK

[2] School of Earth and Environment, University of Leeds, Leeds, LS2 9JT, UK

[3] Departments of Earth Science and Environmental Change, Geography and GIS, and Mechanical Science and Engineering and Ven Te Chow Hydrosystems Laboratory, University of Illinois at Urbana-Champaign, Urbana 61801, USA

ABSTRACT

Understanding of the formative conditions of many sole structures is limited, with chevron marks and striated groove marks being particularly enigmatic. Herein, we examine these sedimentary structures through laboratory modelling. An idealised tool, resembling an armoured mud clast, was dragged through substrates of kaolinite–seawater mixtures of different yield strengths while submerged in seawater. The experiments suggest that armoured mud clasts are the likely tools producing fine striae in striated grooves, and, given the common occurrence of striated groove marks in outcrops, that these clasts are more prevalent in deep-marine settings than previously thought. Chevron marks were observed to form over a narrow range of substrate yield stresses, likely explaining their relative rarity. Furthermore, their form is shown to be a function of substrate rheology, with chevron angle relative to the movement direction of the tool being less in weaker substrates. Moreover, the size of cut chevron marks, characterised by a narrow central cut, bears no relationship to the size of the incising tool, but rather reflects a substrate with a low yield stress that is sufficiently mobile to close behind the tool. In contrast,

26   interrupted chevron marks, characterised by a distinct central groove, reflect greater substrate strength. Striated

27   grooves without chevrons formed at the highest yield stresses simulated in the experiments. The relationship

28   between tool mark type and yield stress, in combination with changes in chevron angle, enables these sole

29   structures to be utilised as indicators of palaeosubstrate rheology. The conditions required to preserve such

30   features include a prolonged period of bed consolidation, flow bypass, and lack of bioturbation. Given changes in

31   seafloor communities and bioturbation over time and their impact on substrate rheology, particularly during the

32   early Palaeozoic, the present work supports the idea that the frequency of these sole structures likely changed over

33   geological time.

34

35   **INTRODUCTION**

36   Sole marks are erosional sedimentary structures formed by the interaction of a flow, or an object present at or near

37   the base of the flow, with a sediment bed, usually consisting of cohesive mud (Dżułyński & Sanders, 1962; Collinson

38   *et al.*, 2006). Their common occurrence and predictable orientation relative to the direction of the flow, or the

39   moving object, has secured sole marks as a prime indicator of palaeoflow direction and orientation in the

40   sedimentary record (*e.g.*, Hall, 1843). More recently, the shape and size of sole marks have been linked with specific

41   types of formative clay-laden flows (Peakall *et al.*, 2020), where: (i) turbulent and turbulence-enhanced flows (*sensu*

42   Baas & Best, 2002; Baas *et al.*, 2009) form scour marks, such as flute marks; (ii) turbulence-attenuated flows form

43   mainly discontinuous tool marks, such as prod marks and skim marks, and; (iii) quasi-laminar plug flows (*sensu* Baas

44   *et al.*, 2009) and fully laminar plug flows (Peakall *et al.*, 2020) generally form continuous tool marks, such as groove

45   marks and chevron marks. However, the formative conditions for many sole structures remain poorly constrained,

46   particularly for chevron marks and striated grooves. Peakall *et al.* (2020) postulated a mechanism for the formation

47   of striated grooves and suggested that the internal striae are formed by clast asperities or potentially armoured

48   mud clasts. Chevron marks have been attributed to shear stress imposed by flows above weak, ductile muds

49   (Dżułyński & Walton, 1965) and the formation of wakes generated around the object, with analogies made to 'bow

50   waves' formed by ships. This link to weak, ductile muds suggests that shape and size of chevron marks are a function

51   of substrate properties.

52   The process-orientated conceptual model of Peakall *et al.* (2020) has been applied to outcrop studies (*e.g.*, Baas *et*

53   *al.*, 2021; Postma *et al.*, 2021; Brooks *et al.*, 2022), but the role of substrate control on sole mark development, and,

54   specifically, the shape and size of striated groove and chevron marks, remains poorly understood. In general, the

55   erodibility of a substrate, and therefore the formation of sole marks, depends on a multitude of physical, chemical,

56   and biological factors (Peakall *et al.*, 2020). These include the shape and size of the impacting tool and the bed

57   properties of mean grain size and size distribution, plasticity index, bulk density, water content, organic matter

58   content, clay mineralogy, bioturbation, concentration of extracellular polymeric substances, and early diagenetic

59   cements. Even though all these factors combine to govern erodibility, bulk density — closely related to water

60   content in mud — exerts the dominant control on erosion in cohesive substrates (Amos *et al.*, 2004; Winterwerp

61   *et al.*, 2012). Here, erodibility is approximated by the yield stress of the substrate, rather than by bed density,

62   because yield stress is independent of clay type. We hypothesise that yield stress governs the shape and size of

63   specific sole marks, and, conversely, that sole marks in sedimentary rocks provide information on the erodibility of

64   the muddy bed during the formation of sole marks. Sole marks may thus present an indirect measure for the

65   rheological characteristics of muddy substrates that is difficult to obtain otherwise.

66   In the present paper, the above-mentioned hypotheses are tested through a series of controlled laboratory

67   experiments using an artificial 'armoured' clast, where the rheology of the bed was altered to assess the role of the

68   substrate on the formation of sole structures. The aims of this paper are to: (1) investigate the effect of mud bed

69   rheology on the formation and preservation state of continuous tool marks; (2) determine the formation

70   mechanism of striated groove marks; (3) delimit the rheological properties of the bed, necessary for the generation

71   and preservation of continuous tool marks, and; (4) determine how the experimental data can be used as a means

72   for interpreting the rheology of muddy substrates in the geological record from the type, size, and shape of

73   continuous tool marks.

74

75   **BACKGROUND**

76   Chevron marks and groove marks are continuous tool marks, as opposed to discontinuous tool marks, such as skim

77   and prod marks (Dżułyński & Sanders, 1962; Peakall *et al.*, 2020). Continuous, often straight, tool marks generally

78   extend beyond the scale of outcrops, as shown by 35-m long groove marks described by Draganits *et al.* (2008). In

79   deep-marine environments, these marks are formed by tools, commonly mud clasts that are carried by the flow

80   (Peakall *et al.*, 2020), whilst in shallow water a wider range of tools is inferred, including woody debris (Lamb *et al.*,

81   2008; Myrow *et al.*, 2008). The nature of these structures and their proposed formative mechanisms are reviewed

82   briefly here.

83   *Chevron marks*

84   Viewed in planform, chevron marks consist of closely-spaced V- or U-shaped ridges that close in the direction of

85   travel (Fig. 1; Dżułyński & Sanders, 1962). Chevron marks can possess V-shaped ridges separated by a central cut

86   (cut chevrons) or groove (interrupted chevrons), or V- or U-shaped ridges that lack any central lineation

87   (uninterrupted chevrons; Figs 1 and 2; Craig & Walton, 1962; Dżułyński & Sanders, 1962). Cut and interrupted

88   chevrons have been linked to a tool that cuts into the substrate, whilst uninterrupted chevrons have been

89   postulated to form from a tool that is not in contact with the bed, but travels at a fixed height above the bed

90   (Dżułyński & Walton, 1965; Peakall *et al.*, 2020). Chevrons are generally narrow, a few millimetres wide (Fig. 2C),

91   although larger widths in the centimetric range are associated with interrupted chevrons (Figs 2B, D). Some

92   chevrons, particularly of centimetric width, may show a distinctive pattern with the downstream end of the ridge

93   being steepest, and folded over on itself (Figs 1 and 3). Although the relative frequency of chevrons has not been

94   documented in the literature, our observations from extensive fieldwork examining sole marks, is that they are

95   comparatively rare, with just a few observed across whole field areas (*e.g.*, Aberystwyth Grits, Wales, Baas *et al.*,

96   2021).

97   Experiments dragging a stick through mud, or a matchstick above a mud bed, generated cut chevrons and

98   uninterrupted chevrons, respectively (Dżułyński & Walton, 1963, 1965; Kelling *et al.*, 2007). Similarly, experiments

99   with plaster-of-Paris flows over weak mud beds, and sand-rich flows over plaster-of-Paris beds, enabled tools to

100   form chevron marks (Dżułyński & Walton, 1963; Dżułyński & Simpson, 1966; Dżułyński, 1996). However, these

101   experiments lacked data on flow and bed rheology, and the authors were unable to elucidate formative

102   mechanisms. In the absence of experimental evidence, there has been debate concerning the mechanisms forming

103   chevron marks. Chevrons have been postulated to form from the shear stress imposed by flows on weak, ductile

104   muds, because of wakes that are analogous to those generated behind ships (Craig & Walton, 1962; Dżułyński &

4

105   Sanders, 1962). Ships form interrupted chevrons in water, as the ship cuts through the bow wave. Later, Dżułyński

106   & Walton (1965) argued that, if a tool cuts the bed, the sediment to the side may form ridges. The exact mechanism,

107   whether physical or fluidal, for creating ridges was not described, although it can be assumed to be fluidal, based

108   on the work of Craig & Walton (1962) and Dżułyński & Sanders (1962). The formative mechanics of uninterrupted

109   chevrons have been debated by Dżułyński & Walton (1965), Allen (1984) and Peakall *et al.* (2020). Dżułyński &

110   Walton (1965) argued for eddying behind a tool, with reduced suction on the substrate as the particle moves away

111   from the bed. In turn, Dżułyński & Walton (1965) posited that this led to a change from V-shaped to U-shaped

112   chevrons. However, Allen (1984) argued that this mechanism was untenable as the tool should travel at a slower

113   rate than the flow, and thus any eddies should advect downstream, not upstream as interpreted from the chevron

114   direction. If, as argued by Peakall *et al.* (2020), the tools are supported in the base of a plug flow, the objections of

115   Allen (1984) are overcome, as the tool travels at the same speed as the flow.

116   *Striated grooves*

117   Grooves in deep-marine systems, where they were initially defined, are remarkably straight, although some gently

118   curve, exhibit constant width and depth, and are typically continuous on the scale of an individual outcrop. Some

119   of these are associated with raised ridges on their flanks (Dżułyński & Walton, 1965), but their margins are typically

120   sharp. Grooves may also possess parallel striae (Dżułyński & Walton, 1965; Allen, 1984; Fig. 2E). Groove widths

121   range from millimetric to several metres and groove depths extend from several millimetres to *c.* 200 mm (Dżułyński

122   & Walton, 1965; Draganits *et al.*, 2008). Few data have been collated on the internal striae of grooves. However,

123   up to tens of striae, with typically millimetric to centimetric spacing, are shown in photographic examples (Peakall

124   *et al.*, 2020; Fig. 2E). In shallow-marine environments, grooves have been defined differently, to include continuous

125   examples, but also shorter, discontinuous features (*e.g.,* Benton & Gray, 1981; Beukes, 1996; Lamb *et al.*, 2008),

126   referred to as bounce or skim marks in the deep-marine literature (Dżułyński & Sanders, 1962; Allen, 1984; Peakall

127   *et al.*, 2020) and sedimentological textbooks (Bridge & Demicco, 2008; Boggs, 2014; Collinson & Mountney, 2019).

128   We herein use the original deep-marine definition for grooves.

129

130   The formation of grooves has been linked to the dragging of tools through a cohesive substrate. However, the

131   nature of the formative flows has remained enigmatic, with a wide range of different flow conditions postulated.

132   Peakall *et al*. (2020) reviewed the formative mechanisms for grooves, and concluded that their constant width,

133   depth, and straightness demonstrate that the tools must have been held rigidly at a constant height, without

134   undergoing rotation, which in turn indicates a flow with cohesive strength. Peakall *et al*. (2020) proposed that

135   grooves were formed by debris flows, or in some cases slumps and slides, with the tools held rigidly to the base of

136   the plug flow. Specifically, grooves were associated with quasi-laminar plug flows or laminar plug flows (Baas *et al*.,

137   2009; Peakall *et al*., 2020), with Peakall *et al.* (2020) suggesting that striated grooves might be the product of clast

138   asperities or armoured mud clasts.

139   *Pristine preservation of chevron marks and striated grooves*

140   The pristine preservation of chevrons and often millimetric striae in outcrops (*e.g.*, Fig. 2; Peakall *et al*., 2020) raises

141   a paradox: How does a flow that transports a tool in a fixed position and drags it through the substrate, not erode

142   these millimetric structures, once formed? Herein, we present a new model for the structure of, and the position

143   of tools in, these formative flows that resolves this paradox.

144

145   **METHODS**

146   The formation of tool marks was modelled in the Hydrodynamics Laboratory of the School of Ocean Sciences,

147   Bangor University, by dragging an object submerged in seawater across a muddy substrate in a rectangular tank,

148   0.115 m wide, 0.674 m long, and 0.153 m high (Fig. 4; Video 1). The tank was filled up to half its height (*c.* 0.076 m)

149   with a homogeneous mixture of kaolin clay (Whitchem China Clay Polwhite E Powder; median grain size: 0.009 mm;

150   density, ρ_s: 2600 kg m^{-3}) and seawater (density, ρ_w: 1027 kg m^{-3}). After flattening the clay surface, seawater was

151   added to a height of *c.* 0.14 m. The seawater was sourced from the Menai Strait, a tidal channel next to the

152   Hydrodynamics Laboratory, and was filtered to remove suspended material before being used in the experiments.

153   Twelve experiments were conducted using bed bulk densities ranging from 1367.7 kg m^{-3} to 1612.2 kg m^{-3} (Table

154   1), equivalent to water contents ranging from 62.8% to 78.3%. At bed densities below 1300 kg m^{-3}, or a water

155   content above 83%, the substrate was unstable because of high rates of consolidation and dewatering.

156   Herein, the yield stress, which is the minimum shear stress required to initiate motion of a clay–water mixture, is

157   used to describe the cohesive strength of the clay beds. Using yield stress instead of bed bulk density removes the

158   need to consider clay type, because, for example, kaolinite is less cohesive than illite at a given concentration in the

159   sediment bed (Hillel, 2004; Yong *et al.*, 2012). Amongst the clay minerals most commonly found in nature, kaolinite

160   is the weakest whilst montmorillonite is the strongest in terms of cation exchange capacity, a parameter used

161   commonly to describe cohesion (*e.g.*, Baker *et al.*, 2017). Baker *et al.* (2017) measured the yield stress of kaolinite

162   and montmorillonite (bentonite), using the same type of kaolinite from the same supplier as in the present

163   experiments (Whitchem China Clay Polwhite E Powder). Using data from Baker *et al.* (2017; table 2), the following

164   best-fit equations were derived for kaolinite (Equation 1) and montmorillonite (Equation 2):

165
$$\tau_y = 3.1 \cdot 10^{-3} C^{3.15} \tag{1}$$

166
$$\tau_y = 6 \cdot 10^{-3} C^{3.05} \qquad \text{for } C \le 18\% \tag{2a}$$
167
$$\tau_y = 90.5 C - 1588 \qquad \text{for } C > 18\% \tag{2b}$$

168   where τ_y is the yield stress and C is the percentage volumetric clay concentration, which can be converted from

169   bed density, ρ_b, using:

170
$$C = 100 \frac{\rho_b - \rho_w}{\rho_s - \rho_w} \tag{3}$$

171   where ρ_w = 1027 kg m^{-3} is the density of seawater and ρ_s is the sediment density: ρ_s = 2600 kg m^{-3} for kaolinite and

172   ρ_s = 2350 kg m^{-3} for montmorillonite. Equations 1–3 were used to show that the range of bed bulk density used in

173   the present experiments (1367.7 kg m^{-3} to 1612.2 kg m^{-3}) corresponds to yield stresses of 50.0 N m^{-2} to 274.7 N m^{-2}

174   ^{2}, and that the bed was unstable at 1300 kg m^{-3} equivalent to τ_y < 24.9 N m^{-2}. In turn, these yield stresses correspond

175   to bulk bed densities of montmorillonite–seawater mixtures of 1266.5 kg m^{-3} to 1299.3 kg m^{-3}, with instability below

176   1230.0 kg m^{-3}.

177   Van Rijn (1993) proposed a classification scheme for natural clay beds based on density limits (Table 2), which is

178   used herein to nominally describe the clay beds. Given the arguments above, it would be more generically useful

179   to define bed types based on yield stress limits. Beds composed of mixtures of different clay mineral types, which

180   include moderately cohesive illite, are more typical in the natural environment than beds composed solely of weakly

181   cohesive kaolinite or strongly cohesive montmorillonite (Baker *et al.*, 2017). As a first approximation, and in the

182   absence of further relevant data, we therefore take the average bed densities for kaolinite and montmorillonite to

183   convert the bed density limits of van Rijn (1993) to yield stress limits (Table 2). This reveals that the experiments

184   mainly covered 'fluid–solid' and 'stiff mud' bed types, which, according to the estimations of van Rijn (1993), take

185   on the order of a year to decades to form by consolidation of a fluid mud (Table 2).

186   The object used in the experiments was a hollow spikey ball filled with wet sand (Fig. 5). The ball had a mass of

187   0.1185 kg and diameter of 0.052 m (volume: 7.5×10^{-5} m^3), and the spikes were 6.5 mm long and 5 mm wide. The

188   ball was placed on the sediment surface and allowed to penetrate the bed under its own weight, and then attached

189   to a fishing reel by means of a thin wire attached to a threaded bolt (Fig. 4), to allow the ball to be dragged manually

190   across the muddy bed at a near-constant dragging speed of 54 ± 16 mm s^{-1}. Each experiment lasted c. 13 seconds,

191   with the choice of velocity allowing the clast to stay in continual contact with the bed. Before commencing each

192   experiment, a small amount of brown bentonite clay was sprinkled in transverse bands onto the white kaolin

193   surface in order to visualise bed deformation caused by movement of the object (Fig. 4). Exceptions were

194   experiments with yield stresses of 50.0 N m^{-2}, 69.1 N m^{-2}, and 91.3 N m^{-2}, in which the bentonite was sprinkled onto

195   the bed uniformly, rather than in distinct bands. After each experiment, the seawater was siphoned out of the tank

196   at a rate slow enough to prevent bed disturbance. Thereafter, the shape and size of the tool mark were recorded

197   using a protractor and calliper gauge. The calliper gauge was also used to record a vertical profile of the tool mark

198   perpendicular to the dragging direction at a horizontal and vertical resolution of 5 mm and 0.1 mm, respectively.

199

200   **RESULTS**

201   **Visual observations of tool mark development and tool mark shape and size**

202   The experimental data reveal considerable changes in tool mark formation mechanism, shape and size, as the yield

203   stress was increased and the bed type changed from fluid mud to stiff mud. These changes were recorded in four

204   different types of tool mark (Fig. 6): (1) wide, low-angle chevron marks with a narrow, central, non-striated groove

205   (Fig. 6A); (2) striated groove marks with pronounced low-angle chevron marks and surficial clay clasts (Figs 6B, C);

206   (3) striated groove marks with narrow, medium- to high-angle chevron marks (Figs 6D, E), and; (4) striated groove

207   marks without chevron marks (Fig. 6F). Before describing each of these types and their formative mechanism in

8

208   detail, it should be noted that the spherical tool produced tool marks only at yield stresses >58.9 N m^{-2}. As

209   mentioned previously, the bed was unstable at <24.9 N m^{-2}, because of high rates of consolidation. A more stable

210   gel developed between 24.9 N m^{-2} and 58.9 N m^{-2}, but these yield stresses were too low to support the tool, which

211   was then largely, or fully, submerged below the bed surface.

212   *Wide, low-angle chevron marks with a narrow, central, non-striated groove (cut chevron marks)*

213   Between yield stresses of 58.9 N m^{-2} and 71.6 N m^{-2}, roughly half of the tool was submerged below the bed surface

214   before it was dragged across the bed. During dragging, clay was displaced sideways and over the top of the tool.

215   Most of this clay filled the groove formed by the moving tool immediately, thus preserving a shallow and narrow

216   groove, up to 5 mm deep and 6 mm wide (Figs 6A and 7A). This groove lacked striae and possessed chevrons that

217   were formed by ductile deformation of the clay away from the surface of the moving tool (Fig. 6A). These chevrons

218   stretched across the entire width of the tank and their angle with respect to the dragging direction was 34°.

219   *Striated groove marks with low-angle chevrons and surficial clay clasts (low-angle interrupted chevron marks)*

220   Combined groove–chevron marks were formed at yield stresses between 71.6 N m^{-2} and 82.8 N m^{-2} (Figs 6B, C). The

221   grooves were wider than the local diameter of the tool at the point where it was cutting the bed, because the side

222   walls of the grooves collapsed behind the moving tool, helped by the large initial depth and steep walls of the

223   grooves (Figs 7B, C). The collapsed sediment was preserved as clay clasts lining the wall of the grooves (Figs 6B, C).

224   These tool marks possessed lateral ridges, up to 5 mm high (Figs 7B, C), formed by accumulation of clay pushed

225   sideways by the moving tool. In contrast to the cut chevron marks, no clay was pushed over the top of the tool and

226   the clay was too cohesive to fill the groove behind the moving tool, except as clasts. The spikes on the spherical

227   tool formed parallel striae in the grooves, but these were partially covered by the clay clasts (Figs 6B, C). The

228   chevrons were similar to those in the cut chevron marks, except for a smaller angle relative to the dragging

229   direction: 25° and 16° at yield stresses of 74.4 N m^{-2} and 79.9 N m^{-2}, respectively. These tool marks are therefore

230   categorised as low-angle interrupted chevron marks.

231   *Striated groove marks with narrow, medium- to high-angle chevrons (high-angle interrupted chevron marks)*

232   These tool marks, which formed at yield stresses between 82.8 N m^{-2} and 158.0 N m^{-2}, were similar to the low-angle

233   interrupted chevron marks, but with notable differences. The chevron angle rapidly increased as the yield stress

234   increased (Figs 6D, E), culminating in an 84° angle, *i.e.,* an almost total lack of chevrons, at 143.7 N m^{-2}. These tool

235   marks are therefore categorised as high-angle interrupted chevron marks. The chevrons narrowed as chevron angle

236   increased, until their width was less than 10 mm at a yield stress of 143.7 N m^{-2}. The striae in the grooves of the

237   high-angle interrupted chevron marks were not covered by clay clasts, and thus the continuous character and

238   sharpness of individual striae were better exposed, when viewed from above (Figs 6D, E). The grooves were also

239   narrower and shallower, and their lateral ridges thinner, than those of the low-angle interrupted chevron marks

240   (Figs 7D–G).

241   *Striated groove marks without chevrons (chevron-less groove marks)*

242   These tool marks, formed at yield stresses between 158.0 N m^{-2} and 274.7 N m^{-2}, were chevron-less groove marks,

243   with small groove widths and shallow groove depths (Figs 6F and 7H–J). These characteristics reflect the shallow

244   initial penetration depth of the tool into these firm substrates. Striae in the groove marks were sharp and perfectly

245   parallel (Fig. 6F), and the lateral ridges had a thickness similar to those in the high-angle interrupted chevron marks.

246   **Geometrical characterization of the tool marks**

247   Characteristic geometrical properties of the experimental tool marks are plotted against yield stress in Fig. 8. Figure

248   8A shows the maximum depth of the grooves and the mean of the maximum thickness of the left-lateral and right-

249   lateral ridges lining the grooves. The maximum depth increased rapidly from 5 mm to 15.5 mm across the boundary

250   between the cut, and low-angle interrupted, chevron marks (Fig. 8A), which was associated with the change from

251   filling of the groove behind the moving tool at τ_y = 69.1 N m^{-2} to unfilled grooves. The low-angle interrupted chevron

252   marks were the deepest of all the tool mark types, with the groove depth of the high-angle interrupted chevron

253   marks gradually decreasing linearly as yield stress increased (Fig. 8A). This trend continued for the chevron-less

254   groove marks, but at a slower rate than for the high-angle interrupted chevron marks. The chevron-less groove

255   marks were only 0.6 mm to 2.7 mm deep (Fig. 8A).

256   The cut chevron marks lacked lateral ridges (Figs 7A and 8A), whereas the deep low-angle interrupted chevron

257   marks had well-developed lateral ridges with a maximum thickness of 3.5 mm and 4.9 mm on each of the two

258   flanks. The shallower, high-angle, interrupted chevron marks and chevron-less groove marks lacked clear trends in

259   lateral ridge thickness (Fig. 8A). The mean thickness for these tool marks was *c.* 2 mm, which is *c.* 50% of the low-

260   angle interrupted chevron mark thickness. Lateral ridges were absent at the highest yield stress of 274.7 N m^{-2} (Fig.

261   8A).

262   Groove mark width (Fig. 8B) shows a proportional relationship to groove mark depth (Fig. 8A); wide groove marks

263   tended to be deep, and narrow groove marks tended to be shallow. Hence, the cut chevron marks had the lowest

264   width, the low-angle interrupted chevron marks had the highest width, and there is an inverse relationship between

265   groove mark width and yield stress for the high-angle interrupted chevron marks and chevron-less groove marks

266   (Fig. 8B). The angle of the chevrons with respect to the tool dragging direction changed with yield stress (Fig. 8C).

267   These angles decreased from 34° to 25° to 16° across the boundary between the cut and low-angle interrupted

268   chevron marks. The low angles of the latter correspond to the large groove depths and widths, and thick lateral

269   ridges of this tool mark type. The high-angle interrupted chevron marks possessed narrower chevrons, with angles

270   that increased from 59° to 84°, as yield stress increased. The bentonite bands were not deformed in the chevron-

271   less groove marks (shown by the 90° angles in Fig. 8C).

272

273   **DISCUSSION**

274   **Origin of chevron marks and striated groove marks**

275   *General remarks*

276   The experimental data support the previous concept that tools dragged across a soft, muddy substrate can form

277   cut chevron marks (Fig. 6A) and interrupted chevron marks (Figs 6B–E) (Dżułyński & Walton, 1963, 1965; Dżułyński

278   & Simpson, 1966; Dżułyński, 1996; Kelling *et al.*, 2007) and that striated grooves are the product of clasts with

279   asperities (Figs 6B–F; Peakall *et al.*, 2020). Uninterrupted chevron marks did not form in the experiments, suggesting

280   that these features are not related to tools cutting the bed. These may instead be related to tools dragged above

281   the bed, as postulated since the 1960s (Craig & Walton, 1962; Dżułyński & Sanders, 1962).

282   *Origin of chevron marks*

283   The present experiments provide novel information concerning the formative mechanisms of cut and interrupted

284   chevron marks as influenced by differences in yield stress of the clay. These improve upon earlier experiments

285   conducted with plaster-of-Paris, for which the yield stresses were not measured (Dżułyński & Walton, 1963;

286   Dżułyński & Simpson, 1966; Dżułyński, 1996). Chevrons formed only in the kaolinite beds at τ_y = 58.9 – 158.0 N m-

287   ^{2}. The chevron marks with a narrow, central groove resemble cut chevron marks, whereas the groove marks with

288   variably angled chevrons resemble interrupted chevron marks (*cf.*, Dżułyński & Walton, 1963, 1965; Dżułyński &

289   Simpson, 1966; Dżułyński, 1996; Kelling *et al.*, 2007). The present experiments show that the cut chevron marks,

290   which formed at a narrow range of yield stresses between 58.9 N m^{-2} and 71.6 N m^{-2}, require water-rich clay beds

291   with a relatively low cohesive strength. We infer that the shear induced by the moving tool was able to deform, re-

292   orientate, and possibly also break the bonds between the kaolinite particles (*cf.*, Philippe *et al.*, 2011). This caused

293   the displaced kaolinite to move around and over the top of the tool like a fluid, quickly filling the groove behind the

294   tool, and preserving the original groove as a shallow, narrow structure. Additionally, more ductile deformation

295   caused the formation of chevron marks away from the centre of shear around the tool, where the clay structure

296   remained largely intact. This stressing of the ductile clay adjacent to the moving tool (Craig & Walton, 1962;

297   Dżułyński & Sanders, 1962) created wide chevrons that extended to the walls of the tank. The low angle of the cut

298   chevron marks is a further indication of the highly ductile properties of the kaolinite–water mixture under these

299   experimental conditions.

300   The interrupted chevron marks, which formed at τ_y = 71.6 – 158.0 N m^{-2}, had wider and generally deeper grooves

301   than the cut chevron marks, because the grooves were not infilled with kaolinite that was pushed sideways and

302   backward by the moving tool, as present in the cut chevron marks. Instead, the clay accumulated predominantly

303   onto lateral ridges (Figs 7B–G; Dżułyński & Walton, 1965). The presence of these lateral ridges, together with the

304   presence of mud clasts that lined the deep grooves, suggests that the cohesive bed strength associated with

305   interrupted chevron marks is greater than for cut chevron marks. However, the low-angle interrupted chevron

306   marks were still sufficiently ductile to form low-angle chevrons that extended to the walls of the tank. In contrast,

307   the high-angle interrupted chevron marks attained a progressively greater chevron angle (Fig. 8C), and a narrower

308   width, as a result of an increase in the yield stress from 82.8 N m^{-2} to 158.0 N m^{-2}. These trends are likely because

309   bed deformation at these higher yield stresses decays more quickly away from the moving tool, and possibly

310   because the tool did not penetrate as deeply into the bed, thus reducing the total amount of shear. The cohesive

311   strength of the bed at yield stresses >158.0 N m^{-2} was too great to allow the formation of chevrons, thus generating

312   chevron-less groove marks. The stability field of these groove marks probably extends beyond the maximum yield

313   stress of 274.7 N m^{-2} investigated herein, although it is likely there is a yield strength above which the bed is too

314   hard to form grooves and their striae. Further research is needed to establish this limit for kaolinite and other clay

315   types, and possibly other tool shapes.

316   Returning to the analogy between chevrons and ship wakes, we note that deep-water ship wakes have a constant

317   angle of 19.5° (Bertram, 2000), close to the minimum angle observed herein for the striated groove marks with

318   pronounced low-angle chevrons (Fig. 8C). In shallower water, ship wake angles increase to up to 90° at a Froude

319   number, $Fr = U/\sqrt{(gh)} = 1$, where U is ship velocity, g is the gravitational constant and h is the water depth, before

320   progressively decreasing again in supercritical conditions ($Fr > 1$; Bertram, 2000). The experimental chevron angles

321   are more analogous to these shallow-water examples of ship wakes than those of ship wakes in deep water.

322   Therefore, chevron mark angle may also be a function of velocity, a parameter not examined in the present study.

323   *Nature of the formative tools in striated grooves*

324   Except for the narrow grooves of the cut chevron marks, striae were preserved and straight (*cf.*, Peakall *et al.*, 2020)

325   in all the grooves. Hence, the formation and preservation of striated grooves is independent of yield stress, provided

326   that the bed can be deformed in a ductile manner. However, striae are particularly well-defined in chevron-less

327   groove marks formed in stiff, high-yield-stress clay, and they are partly covered by mud clasts at the edge of grooves

328   in low-angle interrupted chevron marks.

329   The present experiments therefore demonstrate that tools with asperities form striated grooves, but a key question

330   is what types of tools form striated groove marks in nature? The thin delicate nature of some internal striae, and

331   the large number of striae — typically tens of striae — observed in some outcrop cases, would appear to require

332   an unusual number, and tight spacing, of sharp asperities on the surface of the formative tools. In some cases, striae

333   also appear regularly spaced (Fig. 2E). It is hard to envisage how primary unlithified mud clasts that dominate tools

334   in deep-marine environments (Peakall *et al*., 2020) would exhibit this range of features on account of their initial

335   erosion, or how, if present, such sharp and frequently small asperities would avoid breakage and abrasion during

336   dragging of the clast through the substrate. In shallow-marine environments, woody debris is also unlikely to exhibit

337   such sharp and frequent asperities. Tools comprised of strong asperities that would restrict breakage and abrasion

338   might include diagenetically-produced features such as concretions (*e.g.*, Loope *et al.*, 2012; Pe-Piper & Piper,

339   2020), and armoured mud clasts that roll over a surface whilst acquiring a coating of granular bed material (Li *et*

340   *al.*, 2017), which would provide the asperities. Concretions are typically smooth, although in exceptional cases high

341   numbers of fine asperities can be provided by abrasion of concretions that formed in coarse-grained substrates

342   (*e.g.*, Loope *et al.*, 2012), or by differential cementation of original bedding. However, in deep-marine systems

343   where striated grooves are common, mud clasts are abundant, and gravel-sized tools of non-mud composition,

344   such as concretions, are rare in comparison (Peakall *et al.*, 2020). Armoured mud clasts are therefore expected to

345   be abundant in these settings and striated grooves may give a record of armoured mud clasts that were covered in

346   sand grains. These clasts may be difficult to recognise in the deposits of many deep-water systems, given the

347   restricted spatial variations in grain size that are often present within the sand fraction (*e.g.*, Jobe *et al.*, 2012; Kane

348   *et al.*, 2017; Pierce *et al.*, 2018), thus hindering the distinction between armour sediment and the main sediment

349   in event beds. Examples of armoured mud clasts are known from modern (Gutmacher & Normark, 2002; Stevenson

350   *et al.*, 2018) and ancient (*e.g.*, Stanley, 1964; Mutti & Normark, 1987; Felix *et al.*, 2009; Dodd *et al.*, 2019; Privat *et*

351   *al.*, 2021; Jones *et al.*, 2022; Scarselli, 2023) deep-water clastic systems, with tool diameters ranging from 0.05 m

352   to 0.8 m (Stanley, 1964; Stevenson *et al.*, 2018), and coatings ranging in size from medium- to coarse-grained

353   siliciclastic and bioclastic sand to pebbles (Stanley, 1964; Chun *et al.*, 2002; Privat *et al.*, 2021). Armoured mud clasts

354   are known to be far more resistant to breakage and abrasion than mud clasts without an armour (Hizzett *et al.*,

355   2020) and thus stronger as cutting tools.

356   Given the apparent rarity of concretions with fine asperities, the known examples of armoured mud clasts, and the

357   ubiquity of mudstone clasts in deep-marine clastic systems, it appears that the fine striae of striated grooves might

358   in most cases reflect the transport of armoured mud clasts that have been incorporated into a debris flow, *i.e.*, a

359   quasi-laminar plug flow (see discussion below). Examples of armoured mud clasts are known from both subaqueous

360   debris flows (Chun *et al.*, 2002) and hybrid events (Haughton *et al.*, 2003, 2009; Felix *et al.*, 2009). This interpretation

361   suggests that substantial numbers of striae in grooves indicate the presence of armoured mud clasts, and that the

362   width of the striae can be used to estimate the roughness of the surficial mud clast coating. Armoured mud clasts

363   may therefore be more prevalent in deep-water clastic systems than presently recognised.

364   *A process model for the formation of chevrons and striated grooves*

365   The present experiments demonstrate the importance of tools dragged in fixed positions through substrates with

366   specific rheological properties for the formation of chevrons and striated grooves. The tool marks observed in the

367   experiments are analogous to the pristinely preserved structures observed in the rock record (*e.g.*, Peakall *et al.*,

368   2020). However, the paradox remains as to why a flow with cohesive strength that can transport and drag tools

369   through the substrate, does not simultaneously erode the delicate structures, such as striae and chevrons, that are

370   shown here to form in soft, ductile substrates. Existing knowledge of cohesive flow dynamics can be utilised to

371   resolve this paradox. Quasi-laminar plug flows (debris flows) have been shown to possess a fluidal basal layer

372   beneath the rigid plug (Fig. 9; Baas *et al.*, 2009, 2011; Peakall *et al.*, 2020). Tools, typically clasts, can be envisaged

373   to protrude from the base of the plug flow where they are held in place by cohesive strength. The velocity of the

374   plug flow is greater than that of the fluidal basal layer (Baas *et al.*, 2009, 2011) and thus the tools move through

375   this layer whilst being dragged through the substrate. The fluidal basal layer consists of two parts, a shear zone that

376   exhibits minor residual turbulence, overlying a thickened viscous sublayer at the base of the flow where viscous

377   forces suppress turbulence (Fig. 9). This viscous sublayer was 4–5% of the flow depth (*c.* 6 mm) in the experiments

378   of Baas *et al.* (2009) and, whilst scaling relationships are unknown, Peakall *et al.* (2020) estimated that natural flows

379   likely have viscous sublayers that are tens of millimetres thick, perhaps up to 100 mm. This model explains how

380   tools being dragged through the bed, at velocities of *c.* 1 m s^{-1} (Peakall *et al.*, 2020), can be spatially and temporally

381   related to a near absence of erosion, and therefore the preservation of delicate, at times millimetric, structures in

382   soft, ductile muds. The corollary of this contention is that such sole structures show that the formative flows consist

383   of plug flows riding on a fluidal basal layer with a thickened viscous sublayer, rather than laminar plug flows (*sensu*

384   Peakall *et al.*, 2020), where the plug flow extends all the way to the base of the flow.

385   A second paradox is how the weakest substrates, such as those associated with cut chevrons, are not eroded by

386   the head of the flow prior to the formation of the sedimentary structures. Research on the origin of grooves has

387   argued that in some cases these may be formed by a debritic head (Baas *et al.*, 2021), in keeping with observations

388   from modern currents that the front of the flow has sediment concentrations that can be orders of magnitude

389   higher than the rest of the flow (Azpiroz-Zabala *et al.*, 2017; Pope *et al.*, 2022). In such cases, it is argued that, as a

390   result of a debritic head with an associated thickened viscous sublayer, there can be an absence of erosion of the

391   soft substrate by turbulent or laminar flows. Thus, weak substrates are preserved and cut chevrons can be formed

392   within these. In other cases, such as chevron-less groove marks, the substrate is either more consolidated prior to

393   the arrival of the flow, or the front of the flow was capable of eroding ('stripping off') the uppermost and weakest

394   parts of the substrate prior to the formation of the chevrons, perhaps reflecting some ongoing fluid mixing, and

395   associated erosion, at the front of a debritic head. The corollary of these processes is that chevron marks, and

396   particularly cut chevron marks, are a likely indicator of flows that have debritic heads associated with no, or limited,

397   erosion.

398   The presence of a fluidal basal layer and thickened viscous sublayer in natural quasi-laminar plug flows, and the

399   associated protection of the bed from turbulence and erosion, also suggest that the absence of a flow in the present

400   experiments likely does not cause the structures to develop and be preserved in a significantly different way to

401   those in natural environments.

402   **Is groove width a proxy for tool size?**

403   The experimental data reveal a large variation in the width and depth of the groove marks (Figs 8A, B), suggesting

404   that the value of using groove mark size as a proxy for the diameter of the formative tool is severely limited. This is

405   confirmed by analysis of groove mark width and depth as calculated from the penetration depth of the spherical

406   tool for each yield strength (Fig. 10). For all types of tool mark, groove width is equal to or smaller than the diameter

407   of the tool and the groove depth is smaller than the radius of the tool (Figs 8A, B and 10). These differences are

408   greatest for the cut chevron marks and chevron-less groove marks, because of rapid filling of the groove and shallow

409   tool penetration depths, respectively. Only the groove widths of the interrupted chevron marks approach the tool

410   diameter to within *c.* 7.5% (4 mm) at τ_y = 74.4 – 91.3 N m^{-2} (Fig. 8B). The implication is that groove width can only

411   be used as an approximate representation of tool diameter for interrupted chevron marks, where the chevrons are

412   long and wide relative to the groove width and the angle of the chevrons with respect to the flow direction is low

413   (Fig. 8C). Groove width for all other types of tool mark, as well as the depth of all groove marks, can thus only be

414   used as an indicator of minimum tool diameter.

415   **Tool mark shape as a proxy for substrate yield stress**

416   The present laboratory experiments reveal predictable relationships between tool mark shape and yield stress of

417   kaolinite beds (Fig. 11), which allows the cohesive strength of the bed to be estimated from tool mark shape, with

418   support from tool mark size. The ranges in yield stress (Fig. 11) are within the fluid–solid category of van Rijn (1993)

419   for all the tool mark types with chevrons, whereas groove marks without chevrons extend across the boundary

420   from fluid–solid to firm mud. Moreover, tool marks do not form in fluid mud (at τ_y < 24.9 N m^{-2}), as defined in the

421   classification scheme of van Rijn (1993). The predicted range of yield stresses of 58.9 to 158.0 N m^{-2} for the

422   formation of cut and interrupted chevrons marks is remarkably small and may explain why chevron marks are less

423   common in the geological record than chevron-less groove marks (Enos, 1969; Middleton & Hampton, 1973; Peakall

424   *et al.*, 2020), which are inferred to form at yield stresses exceeding 158.0 N m^{-2}, including in stiff, and possibly hard,

425   mud. The prominence of striae in groove marks may also be an additional qualitative measure to estimate yield

426   stress of the bed at the time of striae formation.

427   In the present experiments, the weight of the tool determined the relative depth to which the tool penetrated the

428   clay bed. However, in natural flows the tool is held at the base of the plug flow, and thus the weight applied to the

429   substrate is that of the plug flow, relative to that of the fluidal basal layer (Fig. 9). In turn, the applied weight

430   determines the depth of incision (Fig. 9), and thus the weight of the clast is not a key variable in controlling

431   penetration depth. However, differences in the applied weight from the overlying plug flow will lead to different

432   penetration depths and thus widths of the chevrons and striated grooves. Whilst penetration depths may vary

433   relative to those observed in the present experiments, the same broad patterns of tool mark width and depth as a

434   function of sole mark type (Fig. 11) and substrate strength are to be expected.

435   **Preservation potential of tool marks**

436   The preservation potential of tool mark types (Fig. 11) may vary with the rheological properties of the bed they are

437   cut into. We postulate that tool marks in mud with a low water content, and thus high yield stress, have a higher

438   preservation potential than those in mud with a high water content. In other words, cut and low-angle interrupted

439   chevron marks in soft mud should possess a lower preservation potential than high-angle interrupted chevron

440   marks, which in turn have a lower preservation potential than chevron-less groove marks formed in stiff mud. This

441   provides further reasoning for the observation that groove marks are more common than chevron marks on the

442   base of sediment beds (Enos, 1969; Middleton & Hampton, 1973; Peakall *et al.*, 2020). In deep-marine

443   environments, yield stresses typical of soft substrates containing tool marks with chevrons (of the order of tens of

444   N m^{-2}; Equation 4) can be overcome by turbidity currents laden with 5% sediment and travelling at 2 to 3 m s^{-1},

445   calculated using the quadratic stress law with a drag coefficient of 0.01 (Parker *et al.*, 1987). Turbidity currents with

446   similar characteristics are common in the modern oceans (*e.g.*, Pope *et al.*, 2022), and thus they likely formed

447   turbidites in the sedimentary record, implying that tool marks with chevrons may be preserved only under specific

448   circumstances (Fig. 12). These include sites where: (a) the flow that forms the tool mark bypasses (*i.e.*, the

449   equilibrium flows of Crisóstomo-Figueroa *et al.*, 2020) the location and there is an extended period without flow

450   across the site afterwards (Peakall *et al.*, 2020; Baas *et al.*, 2021); (b) the seabed has sufficient time to consolidate,

451   thus establishing the 'true substrates' of Davies & Shillito (2021); (c) there is lack of bioturbation, and; (d) the flow

452   that casts the bed is solely depositional, and does not erode these delicate structures. Flow bypass is required

453   because deposited sediment is expected to load into the fluid–solid and destroy any tool marks with chevrons. Bed

454   consolidation leads to an increase in yield strength, thus aiding future tool mark preservation. In the classification

455   scheme of van Rijn (1993), the time needed to progress from a fluid–solid to stiff mud, thereby increasing the

456   preservation potential of the tool marks, is estimated to be of the order of years to decades (Table 2). Bed

457   consolidation and strengthening would enable the substrate to support progressively thicker sand beds without

458   undergoing liquefaction and loading. Consequently, the preservation potential of chevrons that form in the weakest

459   substrates can be postulated to be higher under thinner beds that require shorter timescales between the

460   formation of the sole structures, and subsequent deposition. However, field data to test this contention is currently

461   absent. Furthermore, given their delicate nature, tool marks with chevrons will be destroyed by significant

462   bioturbation, and hence their preservation potential should be greater during dysoxic and anoxic near-bed

463   conditions, when bioturbation is restricted. Lastly, the flow that covers the bed, and casts the structures, needs to

464   be solely depositional (i.e., no associated erosion). Such flows are common in turbiditic systems, associated with

465   flat-based non-erosive sand overlying mud (*e.g.*, Walker & Mutti, 1973; Carlson & Grotzinger, 2001; Brooks *et al.*,

466   2018).

467   The dependence of tool mark characteristics upon substrate type, and particularly the narrow rheological range in

468   which tool marks with chevrons form, also suggests that the abundance of such tool marks may have changed over

469   geological time. A major change in seafloor ecology occurred during the Ordovician, with burrowing becoming more

470   intense (Orr, 2001; Mángano *et al*., 2016). Furthermore, the depth in the bed to which mixing generated by

471   bioturbation occurs increased up to the late Silurian, where it attained a character matching modern conditions

472   (Tarhan, 2018). Thus, greater potential mixing depth and bioturbation intensity may have decreased substrate

473   strength from the Ordovician onwards, thus favouring a higher frequency of tool marks with chevrons. Conversely,

474   however, their preservation may have been hindered by enhanced bioturbation. Chevron-less grooves form over a

475   wider range of firmer substrate rheology, and therefore are less likely to be affected by deposition and deformation

476   immediately after formation, and would be less influenced by bioturbation. Nonetheless, the frequency of

477   formation of different types of groove mark will likely have changed over time, with a greater frequency of harder

478   substrates prior to the late Silurian, which would have favoured the production of chevron-less grooves.

479   In summary, the present experiments suggest that the preservation of tool marks with chevrons requires several

480   conditions (Fig. 12): (1) a soft substrate in the fluid–solid category of van Rijn (1993) at a narrow range of yield

481   stresses; (2) flow bypass; (3) a lack of bioturbation, perhaps encouraged by dysoxic or anoxic conditions; (4)

482   sufficient time for bed consolidation, of the order of years to decades, and; (5) the succeeding flow to be dominantly

483   depositional and unable to erode the chevron marks. Notwithstanding these requirements, the present

484   experiments have shown predictable variations in tool mark shape that can be used to appraise bed densities and

485   yield stresses, and thus bed erodibility and consolidation state, of deposits in the rock record at the time of tool

486   mark formation (Fig. 11).

487

488   **CONCLUSIONS**

489   This study has explored the formative mechanisms of cut and interrupted chevron marks, and striated grooves, to

490   investigate how these provide information on substrate rheology at the time of their formation. Cut chevron marks

491   form in weak mud beds, as the substrate deforms in a fluid-like manner around a tool being dragged through the

492   sediment, filling the groove behind it, and leaving just a narrow groove. The chevrons form by broader deformation

493   to each side of the groove. Interrupted chevrons form in stronger substrates where the central groove is preserved.

494   Striated grooves are likely largely the product of armoured mud clasts, with the depth and spacing of striae

495   recording the roughness of the armouring grains. As substrate yield stress increases, there is a progression from no

496   tool marks, to cut chevrons, interrupted chevrons, striated grooves with chevrons, and finally striated grooves

497   without chevrons. The angle and width of chevron marks also varies with bed yield stress, with cut chevrons forming

498   in a narrow range of bed strengths characterised by a weak fluid–solid rheology. To preserve these delicate

499   structures as sole marks on the base of sandstone beds, we postulate a time gap of the order of years to decades

500   to produce bed consolidation and strengthening prior to deposition of the overlying sand. During this time,

501   bioturbation needs to be absent or limited, perhaps implying anoxic or dysoxic conditions. This knowledge of sole

502   mark type as a function of bed yield stress, can be inverted to interpret palaeosubstrate rheology from chevron and

503   groove types, thus providing a new approach to determining the erodibility of the seabed in deep-marine systems

504   dominated by sediment gravity flows. Combining these results with considerations of the extent of seafloor

505   bioturbation, and its impact on substrate rheology, suggests that the abundance of these sole structures likely

506   changed over geological time. Chevron-less grooves would have been favoured by the harder substrates present

507   prior to the late Silurian. Chevron formation is more likely in weaker substrates, particularly post late-Silurian,

508   although their preservation potential would also likely be lower as a result of enhanced bioturbation.

509

519

520   **REFERENCES**

521   **Allen, J.R.L.** (1984) *Sedimentary Structures: Their Character and Physical Basis*. Elsevier, Amsterdam, 1256 pp.

522   **Amos, C.L., Bergamasco, A., Umgiesser, G., Cappucci, S., Cloutier, D., DeNat, L., Flindt, M., Bonardi, M.** and

523   **Cristante, S.** (2004) The stability of tidal flats in Venice Lagoon—the results of in-situ measurements using two

524   benthic, annular flumes. *Journal of Marine Systems*, **51**, 211–241.

525   **Azpiroz-Zabala, M., Cartigny, M.J.B., Talling, P.J., Parsons, D.R., Sumner, E.J., Clare, M.A., Simmons, S.M., Cooper,**

526   **C.** and **Pope, E.L.** (2017). Newly recognized turbidity current structure can explain prolonged flushing of

527   submarine canyons. *Science Advances*, **3**, e1700200.

528   **Baas, J.H.** and **Best, J.L.** (2002) Turbulence modulation in clay-rich sediment-laden flows and some implications for

529   sediment deposition. *Journal of Sedimentary Research*, **72**, 336–340.

530   **Baas, J.H., Best, J.L., Peakall, J.** and **Wang, M.** (2009) A phase diagram for turbulent, transitional, and laminar clay

531   suspension flows. *Journal of Sedimentary Research*, **79**, 162–183.

532   **Baas, J.H., Best, J.L.** and **Peakall, J.** (2011) Depositional processes, bedform development and hybrid flows in rapidly

533   decelerated cohesive (mud-sand) sediment flows. *Sedimentology*, **58**, 1953–1987.

534   **Baas, J.H., Tracey, N.D.** and **Peakall, J.** (2021) Sole marks reveal deep-marine depositional process and

535   environment: Implications for flow transformation and hybrid-event-bed models. *Journal of Sedimentary*

536   *Research*, **91**, 986–1009.

537   **Baker, M.L., Baas, J.H., Malarkey, J., Silva Jacinto, R., Craig, M.J., Kane, I.A.** and **Barker, S.** (2017) The effect of clay

538   type on the properties of cohesive sediment gravity flows and their deposits. *Journal of Sedimentary Research*,

539   **87**, 1176–1195.

540   **Benton, M.J.** and **Gray, D.I.** (1981) Lower Silurian distal shelf storm-induced turbidites in the Welsh Borders:

541   sediments, tool marks and trace fossils. *Journal of the Geological Society of London*, **138**, 675–694.

542   **Bertram, V.** (2000) *Practical Ship Hydrodynamics*. Butterworth-Heinemann, Oxford, 270 pp.

543   **Beukes, N.J.** (1996) Sole marks and combined-flow storm event beds in the Brixton Formation of the siliciclastic

544   Archean Witwatersrand Supergroup, South Africa. *Journal of Sedimentary Research*, **66**, 567–576.

545   **Boggs Jr, S.** (2014) *Principles of Sedimentology and Stratigraphy, 5th Edition*. Pearson, Harlow, 564 pp.

546   **Bridge, J.S.** and **Demicco, R.V.** (2008) *Earth Surface Processes, Landforms and Sediment Deposits*. Cambridge

547   University Press, Cambridge, 815 pp.

548   **Brooks, H.L., Hodgson, D.M., Brunt, R.L., Peakall, J., Poyatos-Moré, M.** and **Flint, S.S.** (2018) Disconnected

549   submarine lobes as a record of stepped slope evolution over multiple sea-level cycles. *Geosphere*, **14**, 1753–

550   1779.

551   **Brooks, H.L., Ito, M., Zuchuat, V., Peakall, J.** and **Hodgson, D.** (2022) Channel-lobe transition zone development in

552   tectonically-active settings: Implications for hybrid bed development. *The Depositional Record*, **8**, 829–868.

553   **Carlson, J.** and **Grotzinger, J.P.** (2001) Submarine fan environment inferred from turbidite thickness distributions.

554   *Sedimentology*, **48**, 1331–1351.

555   **Chun, S.S., Choe, M.Y.** and **Chough, S.K.** (2002) Armored mudstone boulders in submarine debris-flow deposits,

556   the Hunghae Formation, Pohang Basin: An evidence for the large-scale slumping of adjacent area of a submarine

557   channel or scar wall. *Geosciences Journal*, **6**, 215–225.

558   **Collinson, J.** and **Mountney, N.** (2019) *Sedimentary Structures, 4th Edition*. Dunedin Academic Press, Edinburgh,

559   Scotland, 340 pp.

560   **Collinson, J.**, **Mountney, N.** and **Thompson, D.** (2006) *Sedimentary Structures – 3rd edition*. Terra Publishing,

561   Harpenden, England, 292 pp.

562   **Craig, G.Y.** and **Walton, E.K.** (1962) Sedimentary structures and palaeocurrent directions from the Silurian rocks of

563   Kirkcudbrightshire. *Transactions of the Edinburgh Geological Society*, **19**, 100–119.

564   **Crisóstomo-Figueroa, A., McArthur, A.D., Dorrell, R.M., Amy, L.** and **McCaffrey, W.D**. (2021) A new modelling

565   approach to sediment bypass prediction applied to the East Coast Basin, New Zealand. *Geological Society of*

566   *America Bulletin*, **133**, 1734–1748.

567   **Davies, N.S.** and **Shillito, A.P.** (2021) True substrates: The exceptional resolution and unexceptional preservation

568   of deep time snapshots on bedding surfaces. *Sedimentology*, **68**, 3307–3356.

569   **Dodd, T.J.H., McCarthy, D.J.** and **Richards, P.C.** (2019) A depositional model for deep-lacustrine, partially confined,

570   turbidite fans: early Cretaceous, North Falkland Basin. *Sedimentology*, **66**, 53-80.

571   **Draganits, E., Schlaf, J., Grasemann, B.** and **Argles, T.** (2008) Giant submarine landslide grooves in the

572   Neoproterozoic / Lower Cambrian Phe Formation, Northwest Himalaya: Mechanisms of formation and

573   palaeogeographic implications. *Sedimentary Geology*, **205**, 126–141.

574   **Dżułyński, S.** (1996) Erosional and deformational structures in single sedimentary beds: a genetic commentary.

575   *Annales Societatis Geologorum Poloniae*, **66**, 101–189.

576   **Dżułyński, S.** and **Sanders, J.E.** (1962) Current marks on firm mud bottoms. *Transactions of the Connecticut*

577   *Academy of Arts and Sciences*, **42**, 57–96.

578   **Dżułyński, S.** and **Simpson, F.** (1966) Experiments on interfacial current markings. *Geologica Romana*, **5**, 197–214.

579   **Dżułyński, S.** and **Walton, E.K.** (1963) Experimental production of sole markings. *Transactions of the Edinburgh*

580   *Geological Society*, **19**, 279–305.

581   **Dżułyński, S.** and **Walton, E.K.** (1965) *Sedimentary Features of Flysch and Greywackes*. Developments in

582   Sedimentology 7, Elsevier, Amsterdam, 274 pp.

583   **Enos, P.** (1969) Anatomy of a flysch. *Journal of Sedimentary Petrology*, **39**, 680–723.

584   **Felix, M., Leszczynzki, S., Slaczka, A., Uchman, A., Amy, L.** and **Peakall, J.** (2009) Field expressions of the

585   transformation of debris flows into turbidity currents, with examples from the Polish Carpathians and the French

586   Maritime Alps. *Marine and Petroleum Geology*, **26**, 2011–2020.

587   **Gutmacher, C.E.** and **Normark, W.R.** (2002) Sur submarine landslide, a deep-water sediment slope failure. In:

588   *Submarine Landslides: Selected Studies in the U.S. Exclusive Economic Zone* (Eds W.C. Schwab, H.J. Lee and D.C.

589   Twichell), U.S. Geological Survey, Bulletin 2002, 158–166.

590   **Hall, J.** (1843) *Geology of New York, Part 4, Comprising the Survey of the Fourth Geological District*. Charles Van

591   Benthuyson and Sons, Albany, 683 pp.

592   **Haughton, P.D., Barker, S.P.** and **McCaffrey, W.D.** (2003) 'Linked' debrites in sand-rich turbidite systems — origin

593   and significance. *Sedimentology*, **50**, 459–482.

594   **Haughton, P., Davis, C., McCaffrey, W.** and **Barker, S.** (2009) Hybrid sediment gravity flow deposits classification,

595   origin and significance. *Marine and Petroleum Geology*, **26**, 1900–1918.

596   **Hillel, D.** (2004) *Introduction to Environmental Soil Physics*. Amsterdam, Elsevier Academic Press, 494 pp.

597   **Hizzett, J.L., Sumner, E.J., Cartigny, M.J.B.** and **Clare, M.A.** (2020) Mud-clast armoring and its implications for

598   turbidite systems. *Journal of Sedimentary Research*, **90**, 687–700.

599   **Jobe, Z.R., Lowe, D.R.** and **Morris, W.R.** (2012) Climbing-ripple successions in turbidite systems: depositional

600   environments, sedimentation rates and accumulation times. *Sedimentology*, **59**, 867–898.

601 **Jones, G.E.D., Welbon, A.I.F., Mohammadlou, H., Sakharov, A., Ford, J., Needham, T.** and **Ottesen, C.** (2022)

602 Complex stratigraphic fill of a small, confined syn-rift basin: an Upper Jurassic example from offshore mid-

603 Norway. In: *Cross-Border Themes in Petroleum Geology II: Atlantic Margin and Barents Sea* (Eds D. Chiarella, S.G.

604 Archer, J.A. Howell, C.A.-L. Jackson, H. Kombrink and S. Patruno), Geological Society, London, Special Publication,

605 495, 139–177.

606 **Kane, I.A., Pontén, A.S.M., Vangdal, B., Eggenhuisen, J.T., Hodgson, D.M.** and **Spychala, Y.T.** (2017). The

607 stratigraphic record and processes of turbidity current transformation across deep-marine lobes.

608 *Sedimentology*, **64**, 1236–1273.

609 **Kelling, G., Walton, E.K.** and **Simpson, F.** (2007) The contribution of Stanislaw Dżułyński to flysch sedimentology: A

610 'western' perspective. *Annales Societatis Geologorum Poloniae*, **77**, 93–103.

611 **Lamb, M.P., Myrow, P.M., Lukens, C., Houck, K.** and **Strauss, J.** (2008) Deposits from wave-influenced turbidity

612 currents: Pennsylvanian Minturn Formation, Colorado, U.S.A. *Journal of Sedimentary Research*, **78**, 480–498.

613 **Li, S., Li, S., Shan, X., Gong, C.** and **Yu, X.** (2017) Classification, formation, and transport mechanisms of mud clasts.

614 *International Geology Review*, **59**, 1609–1620.

615 **Loope, D.B.**, **Kettler, R.M., Weber, K.A., Hinrichs, N.L.** and **Burgess, D.T.** (2012) Rinded iron-oxide concretions:

616 Hallmarks of altered siderite masses of both early and late diagenetic origin. *Sedimentology*, **59**, 1769-1781.

617 **Mángano, M.G., Buatois, L.A., Wilson, M.** and **Droser, M.** (2016) The great Ordovician biodiversification event. In:

618 *The Trace-Fossil Record of Major Evolutionary Events* (Eds M.G. Mángano and L.A. Buatois) Springer, Dordrecht,

619 127-156.

620 **Middleton, G.V.** and **Hampton, M.A.** (1973) Sediment gravity flows: Mechanics of flow and deposition. In:

621 *Turbidites and Deep-water Sedimentation* (Eds G.V. Middleton and A.H. Bouma), SEPM Pacific Section short

622 course, 1–38.

623 **Mutti, E.** and **Normark W.R.** (1987) Comparing examples of modern and ancient turbidite systems: Problems and

624 concepts. In: *Marine Clastic Sedimentology: Concepts and Case Studies* (Eds J.K. Legget and G.G. Zuffa), Springer,

625 Dordrecht, 1–38.

626   **Myrow, P.M., Lukens, C., Lamb, M.P., Houck, K.** and **Strauss, J.** (2008) Dynamics of a transgressive prodeltaic

627   system: Implications for geography and climate within a Pennsylvanian intracratonic basin, Colorado, U.S.A.

628   *Journal of Sedimentary Research*, **78**, 512–528.

629   **Orr, P.J.** (2001) Colonization of the deep-marine environment during the early Phanerozoic: The ichnofaunal record.

630   *The Geological Journal*, **36**, 265–278.

631   **Parker, G., Garcia, M., Fukushima, Y.** and **Yu, W.** (1987) Experiments on turbidity currents over an erodible bed.

632   *Journal of Hydraulic Research*, **25**, 123–147.

633   **Pe-Piper, G.** and **Piper, D.J.W.** (2020) Significance of the chemistry and morphology of diagenetic siderite in clastic

634   rocks of the Mesozoic Scotian Basin. *Sedimentology*, **67**, 782-809.

635   **Peakall, J., Best, J.L., Baas, J., Hodgson, D.M., Clare, M.A., Talling, P.J., Dorrell, R.M.** and **Lee, D.R.** (2020) An

636   integrated process-based model of flutes and tool marks in deep-water environments: implications for

637   palaeohydraulics, the Bouma sequence, and hybrid event beds. *Sedimentology*, **67**, 1601–1666.

638   **Philippe, A.M., Baravian, C., Imperor-Clerc, M., De Silva, J., Paineau, E., Bihannic, I., Davidson, P., Meneau, F.,**

639   **Levitz, P.** and **Michot, L.J.** (2011) Rheo-SAXS investigation of shear-thinning behaviour of very anisometric

640   repulsive disc-like clay suspensions. *Journal of Physics: Condensed Matter*, **23**, 194112.

641   **Pierce, C.S., Haughton, P.D.W., Shannon, P.M., Pulham, A.J., Barker, S.P.** and **Martinsen, O.J.** (2018) Variable

642   character and diverse origin of hybrid event beds in a sandy submarine fan system, Pennsylvanian Ross

643   Sandstone Formation, western Ireland. *Sedimentology*, **65**, 952–992.

644   **Pope, E.L., Cartigny, M.J.B., Clare, M.A., Talling, P.J., Lintern, D.G., Vellinga, A., Hage, S., Açikalin, S., Bailey, L.,**

645   **Chapplow, N., Chen, Y., Eggenhuisen, J.T., Hendry, A., Heerema, C.J., Heijnen, M.S., Hubbard, S.M., Hunt, J.E.,**

646   **McGhee, C., Parsons, D.R., Simmons, S.M., Stacey, C.D.** and **Vendettuoli, D.** (2022) First source-to-sink

647   monitoring shows dense head controls sediment flux and runout in turbidity currents. *Science Advances*, **8**,

648   eabj3220.

649   **Postma, G., Lang, J., Hoyal, D.C., Fedele, J.J., Demko, T., Abreu, V.** and **Pederson, K.H.** (2021) Reconstruction of

650   bedform dynamics controlled by supercritical flow in the channel–lobe transition zone of a deep-water delta

651   (Sant Llorenç del Munt, north-east Spain, Eocene). *Sedimentology*, **68**, 1674–1697.

652   **Privat, A.M-L., Hodgson, D.M., Jackson, C.A-L., Schwarz, E.** and **Peakall, J**. (2021) Evolution from syn-rift carbonates

653   to early post-rift deep-marine intraslope lobes: the role of rift basin physiography on sedimentation patterns.

654   *Sedimentology*, **68**, 2563–2605.

655   **Scarselli, N.** (2023) Exploring the predictive power of seismic geomorphology to assess sedimentary characteristics

656   of gravity-flow deposits: examples from offshore East and West Africa reservoirs. In: *Seismic Geomorphology:*

657   *Subsurface Analyses, Data Integration and Palaeoenvironment Reconstructions* (Eds A.M.W. Newton, K.J.,

658   Andresen, K.J. Blacker, R. Harding and E. Lebas), Geological Society, London, Special Publications, 525,

659   https://doi.org/10.1144/SP525-2021-58

660   **Stanley, D.J.** (1964) Large mudstone-nucleus sandstone spheroids in submarine channel deposits. *Journal of*

661   *Sedimentary Petrology*, **34**, 672–676.

662   **Stevenson, C.J., Feldens, P., Georgiopoulou, A., Schönke, M., Krastel, S., Piper, D.J.W., Lindhorst, K.** and **Mosher,**

663   **D.** (2018) Reconstructing the sediment concentration of a giant submarine gravity flow. *Nature Communications*,

664   **9**, 2616.

665   **Tarhan, L.G.** (2018) The early Paleozoic development of bioturbation — Evolutionary and geobiological

666   consequences. *Earth Science Reviews*, **178**, 177-207.

667   **van Rijn, L.C.** (1993) *Principles of Sediment Transport in Rivers, Estuaries and Coastal Seas*. Amsterdam, Aqua

668   Publications, 700 pp.

669   **Walker, R.G.** and **Mutti, E.** (1973) Part IV – Turbidite facies and facies associations. In: *Turbidites and Deep Water*

670   *Sedimentation* (Eds G.V. Middleton and A.H. Bouma), SEPM Pacific Section short course, 119-158.

671   **Winterwerp, J.C., van Kesteren, W.G.M., van Prooijen, B.** and **Jacobs, W.** (2012) A conceptual framework for shear

672   flow–induced erosion of soft cohesive sediment beds. *Journal of Geophysical Research: Oceans*, **117**, C10020.

673   **Yong, R.N., Nakano, M.** and **Pusch, R.** (2012) *Environmental Soil Properties and Behaviour*. London, CRC Press,

674   455 pp.

675

676   **Table 1.** Experimental parameters.

Run	Bed bulk density kaolinite (kg m^{-3})	Yield stress (N m^{-2})	Tool mark type	Chevrons?	Grooves?	Striae?	Predicted bed bulk density montmorillonite (kg m^{-3})
1	1367.7	50.0	none	-	-	-	1266.5
2	1404.7	69.1	1	yes	narrow	no	1269.3
3	1413.6	74.4	2	yes	yes	yes	1270.0
4	1422.4	79.9	2	yes	yes	yes	1270.8
5	1431.0	85.5	3	yes	yes	yes	1271.6
6	1439.5	91.3	3	yes	yes	yes	1272.5
7	1472.4	116.2	3	yes	yes	yes	1276.1
8	1503.5	143.7	3	yes	yes	yes	1280.2
9	1532.8	173.5	4	no	yes	yes	1284.5
10	1560.7	205.4	4	no	yes	yes	1289.2
11	1587.1	239.2	4	no	yes	yes	1294.1
12	1612.2	274.7	4	no	yes	yes	1299.3

677

678   **Table 2.** Clay-bed type classification scheme of van Rijn (1993), showing estimated bed yield stress.

679

Clay-bed type	Wet bulk densities (kg m^{-3})	Estimated yield stresses (N m^{-2})	Consolidation stage	Typical period of consolidation
Dilute fluid mud	1000–1050	0–0.021	Freshly consolidated	1 day
Bingham-type fluid mud	1050–1150	0.021–3.70	Weakly consolidated	1 week
Dense fluid mud	1150–1250	3.70–23.1	Medium consolidated	1 month
Fluid–solid	1250–1350	23.1–331	Highly consolidated	1 year
Stiff mud	1350–1400	331–515	Stiff solid	10 years
Hard mud	>1400	>515	Hard solid	100 years

680   Note: Estimated yield stresses are based on calculating the yield stress for the given bed density for each of
681   kaolinite (a 'weak' clay) and montmorillonite (a 'strong' clay), and taking the average of the two; see text for
682   further details.

683

684   **VIDEO AND FIGURE CAPTIONS**

685

686   **Video 1.** Example of tool mark formation experiment. Yield stress: 79.9 N m^{-2} (Run 4 in Table 1).

687   **Fig. 1.** Schematic diagram showing three different chevron types as seen in planform view (upper), and flow-parallel

688   cross-section for uninterrupted chevrons (lower). Modified after Allen (1984).

689   **Fig. 2.** Field examples of continuous tool marks. (**A**) V-shaped, uninterrupted chevron marks (from experiments in

690   plaster-of-Paris, Jagiellonian University, Kraków, Poland). Chevrons are *c.* 20 mm wide. (**B**) Cut chevron marks with

691   a narrow groove, similar to the chevron marks formed at yields stresses between 58.9 N m^{-2} and 71.6 N m^{-2} in the

692   present study (Bude Formation, North Devon, UK). Scale bar is 20 mm long. (**C**) Interrupted chevron marks with

693   short, high-angle chevrons, similar to the chevron marks formed at yields stresses between 82.8 N m^{-2} and 158.0 N

694   m^{-2} in the present study (Cloridorme Formation, Gaspé Peninsula, Canada). Lens cap for scale. (**D**) Interrupted

695   chevron marks with long, low-angle chevrons, similar to the chevron marks formed at yields stresses between 71.6

696   N m^{-2} and 82.8 N m^{-2} in the present study (Cloridorme Formation, Gaspé Peninsula, Canada). Lens cap for scale. (**E**)

697   Chevron-less groove mark with distinct parallel striae, similar to the chevron marks formed at yield stresses

698   between 158.0 N m^{-2} and 274.7 N m^{-2} in the present study (southern Poland). Yellow bar is 100 mm long.

699   **Fig. 3**. Left-hand tool mark: Interrupted chevron marks with downstream end of the ridges being steepest and

700   folded over on itself. Right-hand tool mark: Chevron-less, striated groove mark. Flow was from top to bottom of

701   image. Scale on top of card is in centimetres. Photograph kindly provided by Lauren Birgenheier, University of Utah.

702   **Fig. 4.** Schematic drawing of the experimental setup as seen in planform. Note that the bentonite bands represent

703   a surficial layer of bentonite overlying the kaolin clay. The tool is dragged from right to left.

704   **Fig. 5.** Spikey, spherical tool (diameter = 0.052 m) used in the experiments.

705   **Fig. 6.** Principal types of experimental tool mark. (**A**) Cut chevron marks: Chevron marks with narrow, central, non-

706   striated groove mark at yield stress τ_b = 69.1 N m^{-2}. (**B**) Low-angle interrupted chevron marks: Striated groove mark

707   with pronounced chevron marks and surficial mud clasts at τ_b = 74.4 N m^{-2}. (**C**) Low-angle interrupted chevron

708   marks: Striated groove mark with pronounced chevron marks and surficial mud clasts at τ_b = 79.9 N m^{-2}. (**D**) High-

709   angle interrupted chevron marks: Striated groove mark with medium-angle chevron marks at τ_b = 85.5 N m^{-2}. (**E**)

710   High-angle interrupted chevron marks: Striated groove mark with weakly developed chevron marks at τ_b = 116.2 N

711   m^{-2}. (**F**) Chevron-less groove mark: Narrow striated groove mark without chevron marks at τ_b = 239.2 N m^{-2}.

712   **Fig. 7.** Cross-sectional profiles perpendicular to the direction of movement of the tool for different bed yield

713   stresses. (**A**) Cut chevron mark; (**B, C**) Low-angle interrupted chevron marks; (**D–G**) High-angle interrupted chevron

714   marks; (**H–J**) Chevron-less groove marks.

715   **Fig. 8.** Geometrical properties of the experimental tool marks as a function of bed yield stress. (**A**) Maximum groove

716   mark depth (blue) and mean of maximum height of left-lateral and right-lateral ridges of groove marks (red). (**B**)

717   Groove mark width. (**C**) Chevron angle with respect to tool dragging direction, where the blue vertical lines

718   represent the standard deviation of the mean and 90° signifies absence of chevrons. Vertical dashed lines and

719   schematic drawings at top of figure refer to tool mark types (from left to right): cut chevron mark; low-angle

720   interrupted chevron mark; high-angle interrupted chevron mark; chevron-less groove mark.

721   **Fig. 9.** Schematic model of a quasi-laminar debris flow with armoured mud clasts attached to the base of the plug

722   and penetrating through the underlying fluidal basal layer (FBL) that has a thickened viscous sublayer (vsl). Pristine

723   preservation of the delicate, often millimetric chevrons and striae, is achieved because the plug flow of the debris

724   flow sits above a fluidal basal layer, the lower part of which is the thickened viscous sub-layer. Clasts attached to

725   the base of the plug flow form grooves and chevrons as they are dragged through the bed, but otherwise turbulence

726   from the flow does not reach the bed. The flow velocity is constant in the plug and rapidly decreases to zero from

727   the top to base of the FBL. Modified after Peakall *et al.* (2020).

728   **Fig. 10.** Groove mark width and depth, as calculated from the observed penetration depth of the spherical tool,

729   against bed yield stress. The tool diameter and radius are given for comparison. Vertical dashed lines and schematic

730   drawings at top of figure refer to tool mark types (from left to right): cut chevron mark; low-angle interrupted

731   chevron mark; high-angle interrupted chevron mark; chevron-less groove mark.

732   **Fig. 11.** Conceptual model of tool mark type in relation to substrate yield stress.

733   **Fig. 12**. Preservation mechanism of cut chevron marks. A prolonged period of quiescence and anoxia or dysoxia,

734   followed by deposition of sand from, for example, a turbidity current is required to preserve these tool marks in

735   natural environments. A similar model applies to low-angle interrupted chevron marks, which also form in mud

736   with a soft fluid–solid rheology (van Rijn, 1993). Note that striae caused by asperities, such as those on armoured

737   mud clasts, do not show in cut chevron marks. Hence, smooth clasts, rather than the armoured clast shown in the

738   left-hand drawing, would produce the same type of chevron marks.

Table 1. Experimental parameters.

Run	Bed bulk density kaolinite (kg m^{-3})	Yield stress (N m^{-2})	Tool mark type	Chevrons?	Grooves?	Striae?	Predicted bed bulk density montmorillonite (kg m^{-3})
1	1367.7	50.0	none	-	-	-	1266.5
2	1404.7	69.1	1	yes	narrow	no	1269.3
3	1413.6	74.4	2	yes	yes	yes	1270.0
4	1422.4	79.9	2	yes	yes	yes	1270.8
5	1431.0	85.5	3	yes	yes	yes	1271.6
6	1439.5	91.3	3	yes	yes	yes	1272.5
7	1472.4	116.2	3	yes	yes	yes	1276.1
8	1503.5	143.7	3	yes	yes	yes	1280.2
9	1532.8	173.5	4	no	yes	yes	1284.5
10	1560.7	205.4	4	no	yes	yes	1289.2
11	1587.1	239.2	4	no	yes	yes	1294.1
12	1612.2	274.7	4	no	yes	yes	1299.3

Table 2. Clay-bed type classification scheme of van Rijn (1993), showing estimated bed yield stress.

Clay-bed type	Wet bulk densities (kg m^{-3})	Estimated yield stresses (N m^{-2})	Consolidation stage	Typical period of consolidation
Dilute fluid mud	1000–1050	0–0.021	Freshly consolidated	1 day
Bingham-type fluid mud	1050–1150	0.021–3.70	Weakly consolidated	1 week
Dense fluid mud	1150–1250	3.70–23.1	Medium consolidated	1 month
Fluid–solid	1250–1350	23.1–331	Highly consolidated	1 year
Stiff mud	1350–1400	331–515	Stiff solid	10 years
Hard mud	>1400	>515	Hard solid	100 years

Note: Estimated yield stresses are based on calculating the yield stress for the given bed density for each of kaolinite (a 'weak' clay) and montmorillonite (a 'strong' clay), and taking the average of the two; see text for further details.
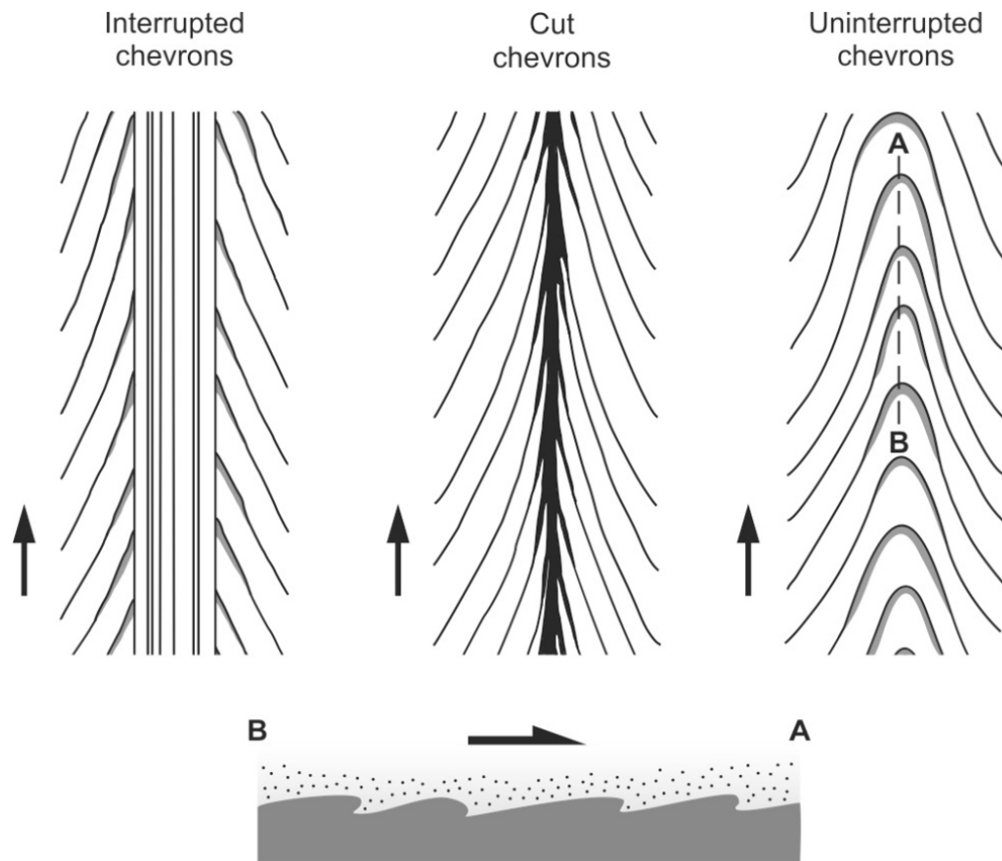
Schematic diagram showing three different chevron types as seen in planform view (upper), and flow-parallel cross-section for uninterrupted chevrons (lower). Modified after Allen (1984).

114x97mm (220 x 220 DPI)

Field examples of continuous tool marks. (A) V-shaped, uninterrupted chevron marks (from experiments in plaster-of-Paris, Jagiellonian University, Kraków, Poland). Chevrons are c. 20 mm wide. (B) Cut chevron marks with a narrow groove, similar to the chevron marks formed at yields stresses between 58.9 N m^{-2} and 71.6 N m^{-2} in the present study (Bude Formation, North Devon, UK). Scale bar is 20 mm long. (C) Interrupted chevron marks with short, high-angle chevrons, similar to the chevron marks formed at yields stresses between 82.8 N m^{-2} and 158.0 N m^{-2} in the present study (Cloridorme Formation, Gaspé Peninsula, Canada). Lens cap for scale. (D) Interrupted chevron marks with long, low-angle chevrons, similar to the chevron marks formed at yields stresses between 71.6 N m^{-2} and 82.8 N m^{-2} in the present study (Cloridorme Formation, Gaspé Peninsula, Canada). Lens cap for scale. (E) Chevron-less groove mark with distinct parallel striae, similar to the chevron marks formed at yields stresses between 158.0 N m^{-2} and 274.7 N m^{-2} in the present study (southern Poland). Yellow bar is 100 mm long.

187x324mm (300 x 300 DPI)

Left-hand tool mark: Interrupted chevron marks with downstream end of the ridges being steepest and folded over on itself. Right-hand tool mark: Chevron-less, striated groove mark. Flow was from top to bottom of image. Scale on top of card is in centimetres. Photograph kindly provided by Lauren Birgenheier, University of Utah.
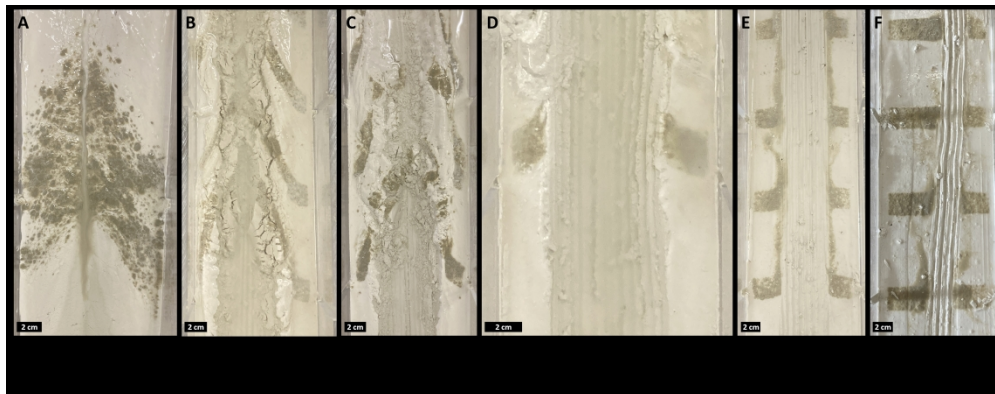
1422x1066mm (72 x 72 DPI)
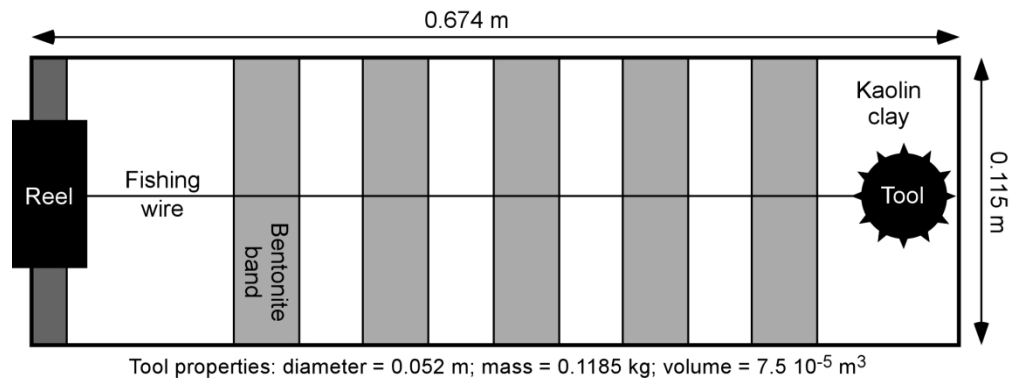
Schematic drawing of the experimental setup as seen in planform. Note that the bentonite bands represent a surficial layer of bentonite overlying the kaolin clay. The tool is dragged from right to left.

180x67mm (300 x 300 DPI)

Spikey, spherical tool (diameter = 0.052 m) used in the experiments.

173x171mm (72 x 72 DPI)

Principal types of experimental tool mark. (A) Cut chevron marks: Chevron marks with narrow, central, non-striated groove mark at yield stress τ b = 69.1 N m^{-2}. (B) Low-angle interrupted chevron marks: Striated groove mark with pronounced chevron marks and surficial mud clasts at τ b = 74.4 N m^{-2}. (C) Low-angle interrupted chevron marks: Striated groove mark with pronounced chevron marks and surficial mud clasts at τ b = 79.9 N m^{-2}. (D) High-angle interrupted chevron marks: Striated groove mark with medium-angle chevron marks at τ b = 85.5 N m^{-2}. (E) High-angle interrupted chevron marks: Striated groove mark with weakly developed chevron marks at τ b = 116.2 N m^{-2}. (F) Chevron-less groove mark: Narrow striated groove mark without chevron marks at τ b = 239.2 N m^{-2}.

335x131mm (330 x 330 DPI)
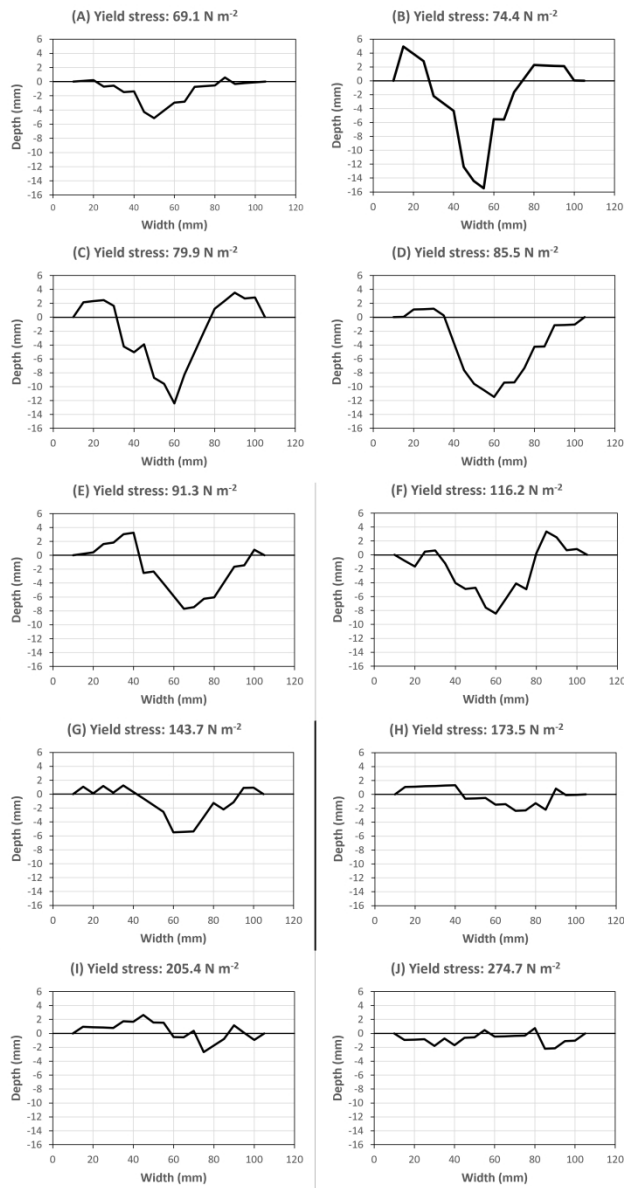
Cross-sectional profiles perpendicular to the direction of movement of the tool for different bed yield stresses. (A) Cut chevron mark; (B, C) Low-angle interrupted chevron marks; (D–G) High-angle interrupted chevron marks; (H–J) Chevron-less groove marks.

207x386mm (330 x 330 DPI)
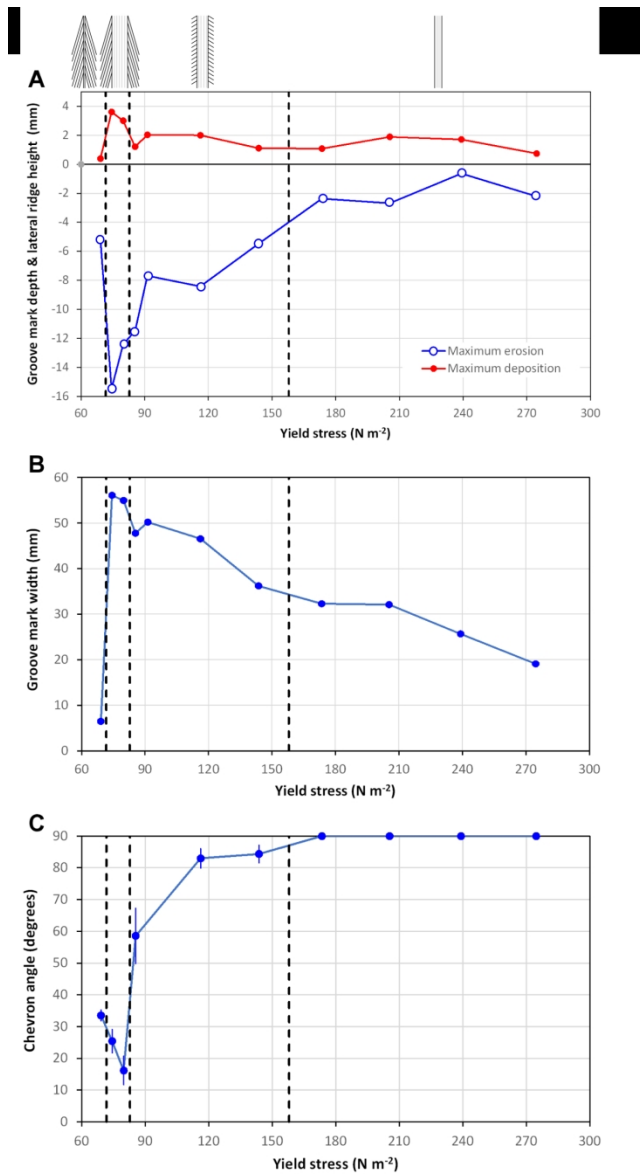
Geometrical properties of the experimental tool marks as a function of bed yield stress. (A) Maximum groove mark depth (blue) and mean of maximum height of left-lateral and right-lateral ridges of groove marks (red). (B) Groove mark width. (C) Chevron angle with respect to tool dragging direction, where the blue vertical lines represent the standard deviation of the mean and 90° signifies absence of chevrons. Vertical dashed lines and schematic drawings at top of figure refer to tool mark types (from left to right): cut chevron mark; low-angle interrupted chevron mark; high-angle interrupted chevron mark; chevron-less groove mark.
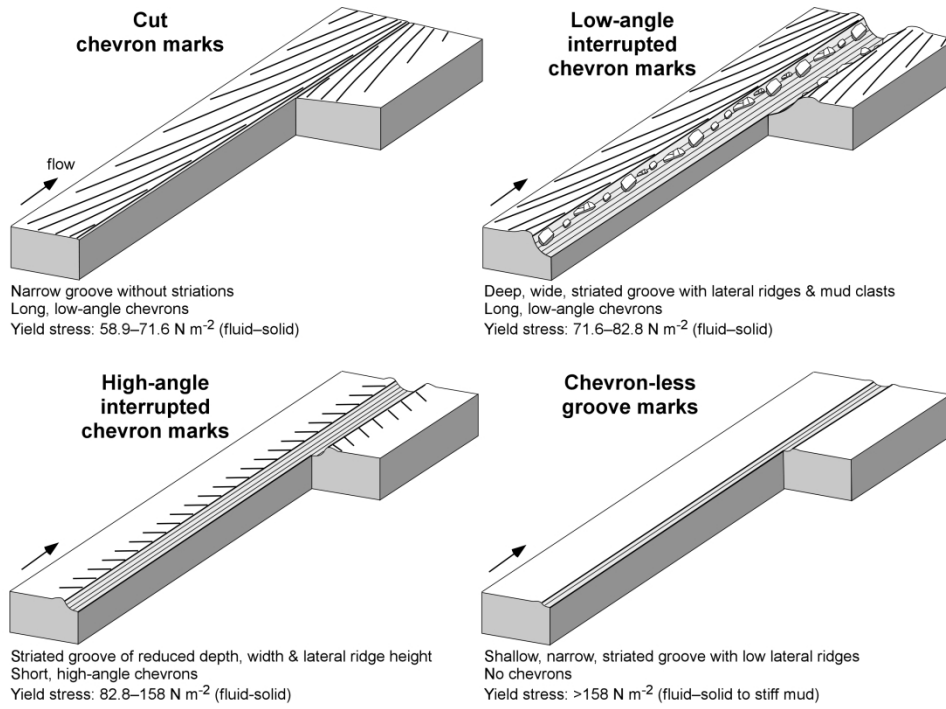
104x195mm (330 x 330 DPI)
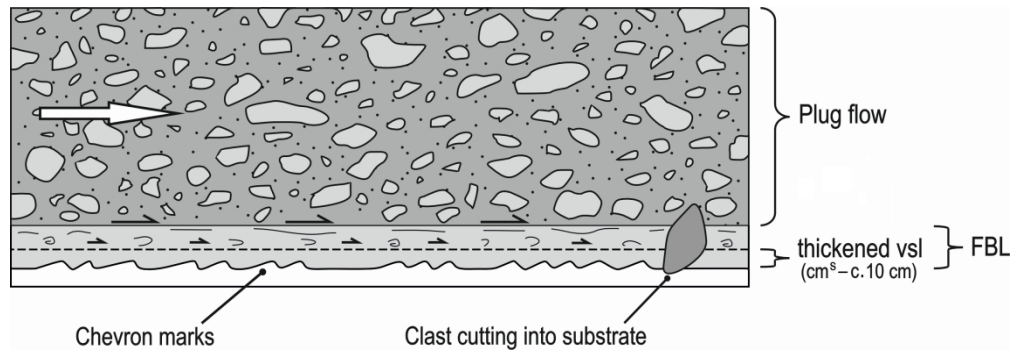
Schematic model of a quasi-laminar debris flow with armoured mud clasts attached to the base of the plug and penetrating through the underlying fluidal basal layer (FBL) that has a thickened viscous sublayer (vsl). Pristine preservation of the delicate, often millimetric chevrons and striae, is achieved because the plug flow of the debris flow sits above a fluidal basal layer, the lower part of which is the thickened viscous sub-layer. Clasts attached to the base of the plug flow form grooves and chevrons as they are dragged through the bed, but otherwise turbulence from the flow does not reach the bed. Modified after Peakall et al. (2020).

750x257mm (96 x 96 DPI)
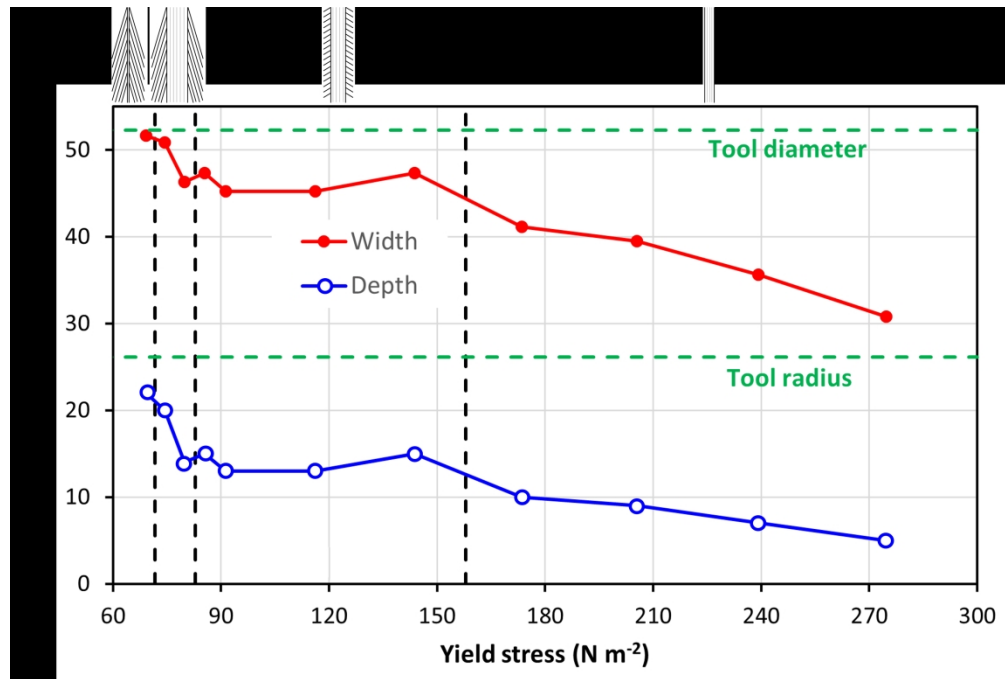
Groove mark width and depth, as calculated from the observed penetration depth of the spherical tool, against bed yield stress. The tool diameter and radius are given for comparison. Vertical dashed lines and schematic drawings at top of figure refer to tool mark types (from left to right): cut chevron mark; low-angle interrupted chevron mark; high-angle interrupted chevron mark; chevron-less groove mark.

246x166mm (330 x 330 DPI)

**Cut
chevron marks**

flow

Narrow groove without striations
Long, low-angle chevrons
Yield stress: 58.9–71.6 N m^{-2} (fluid–solid)

**Low-angle
interrupted
chevron marks**

Deep, wide, striated groove with lateral ridges & mud clasts
Long, low-angle chevrons
Yield stress: 71.6–82.8 N m^{-2} (fluid–solid)

**High-angle
interrupted
chevron marks**

Striated groove of reduced depth, width & lateral ridge height
Short, high-angle chevrons
Yield stress: 82.8–158 N m^{-2} (fluid-solid)

**Chevron-less
groove marks**

Shallow, narrow, striated groove with low lateral ridges
No chevrons
Yield stress: >158 N m^{-2} (fluid–solid to stiff mud)

Conceptual model of tool mark type in relation to substrate yield stress.

269x188mm (300 x 300 DPI)
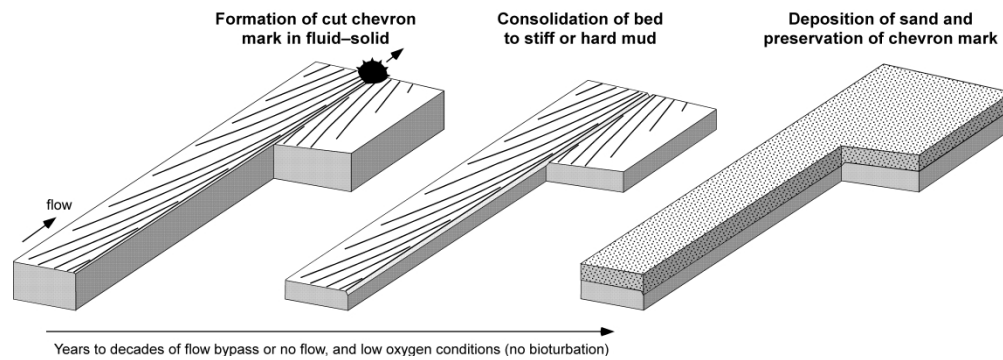
Preservation mechanism of cut chevron marks. A prolonged period of quiescence and anoxia or dysoxia, followed by deposition of sand from, for example, a turbidity current is required to preserve these tool marks in natural environments. A similar model applies to low-angle interrupted chevron marks, which also form in mud with a soft fluid–solid rheology (van Rijn, 1993). Note that striae caused by asperities, such as those on armoured mud clasts, do not show in cut chevron marks. Hence, smooth clasts, rather than the armoured clast shown in the left-hand drawing, would produce the same type of chevron marks.

295x102mm (600 x 600 DPI)